J Mater Sci: Mater Med (2010) 21:1091–1098
DOI 10.1007/s10856-009-3956-1

Bio-corrosion characterization of Mg–Zn–X (X = Ca, Mn, Si) alloys for biomedical applications

F. Rosalbino · S. De Negri · A. Saccone · E. Angelini · S. Delfino

Received: 1 September 2009 / Accepted: 25 November 2009 / Published online: 18 December 2009

Abstract The successful applications of magnesium-based alloys as biodegradable orthopedic implants are mainly inhibited due to their high degradation rates in physiological environment. This study examines the bio-corrosion behaviour of Mg–2Zn–0.2X (X = Ca, Mn, Si) alloys in Ringer's physiological solution that simulates bodily fluids, and compares it with that of AZ91 magnesium alloy. Potentiodynamic polarization and electrochemical impedance spectroscopy results showed a better corrosion behaviour of AZ91 alloy with respect to Mg–2Zn–0.2Ca and Mg–2Zn–0.2Si alloys. On the contrary, enhanced corrosion resistance was observed for Mg–2Zn–0.2Mn alloy compared to the AZ91 one: Mg–2Zn–0.2Mn alloy exhibited a four-fold increase in the polarization resistance than AZ91 alloy after 168 h exposure to the Ringer's physiological solution. The improved corrosion behaviour of the Mg–2Zn–0.2Mn alloy with respect to the AZ91 one can be ascribed to enhanced protective properties of the $Mg(OH)_2$ surface layer. The present study suggests the Mg–2Zn–0.2Mn alloy as a promising candidate for its applications in degradable orthopedic implants, and is worthwhile to further investigate the in vivo corrosion behaviour as well as assessed the mechanical properties of this alloy.

F. Rosalbino (✉) · E. Angelini
Dipartimento di Scienza dei Materiali e Ingegneria Chimica, Politecnico di Torino, Corso Duca degli Abruzzi 24, 10129 Torino, Italy
e-mail: francesco.rosalbino@polito.it

S. De Negri · A. Saccone · S. Delfino
Dipartimento di Chimica e Chimica Industriale, Università degli Studi di Genova, Via Dodecaneso 31, 16146 Genova, Italy

1 Introduction

Due to their high strength, ductility and good corrosion resistance, metallic materials, including stainless steels, titanium alloys and cobalt-based alloys represent an important class of materials in hard tissue replacement, especially load-bearing implants for the repair or replacement of diseased or damaged tissues. However, these metallic materials are not biodegradable in the human body and can cause long-term complications (infection); as a consequence, a second surgical procedure may be necessary after the tissues have healed. Thus, a new domain of research in metallic implants focuses on biodegradable implants, which dissolve in biological environment after a certain time of functional use. Biodegradable implants represent an appropriate solution because of cost, convenience and aesthetic reasons favorable to patients. Magnesium as a biodegradable implant material provides both biocompatibility and suitable mechanical properties. Mg^{2+} ion is present in large amount in the human body, being involved in many metabolism reactions and biological mechanisms, and Mg^{2+} in eccess can be easily excreted in the urine. Moreover, compared to current implant materials, magnesium and magnesium-based alloys have a lower elastic modulus (about 45 GPa which is closed to that of natural bone (10–40 GPa)) and a higher yield strength, that provide them with the potential for avoiding the stress shielding effects [1–3]. Previous in vivo studies have shown that magnesium is suitable as degradable biomaterial for use in medical implants [4, 5].

From a corrosion perspective, magnesium is one of the most active elements and, as well as its alloys, it corrodes rapidly in water-containing media except in the pH alkaline range; a corrosion rate of 10.5–210 mm per year has been indicated for Mg with purity of 99.9% in 3% NaCl solution, relevant for biomedical applications [6]. The poor

corrosion resistance seriously limits the use of Mg and its alloys as permanent metallic implants, but it is a good starting point to consider them for potential applications as bioabsorbable implants. Nevertheless their corrosion performance has still to be improved, in order to better control their degradation time and avoid a too rapid production of hydrogen gas during the corrosion process, which may not be tolerated by host tissues [7, 8].

Recently, a number of studies have been carried out to investigate the corrosion behaviour of magnesium alloys in artificial physiological fluids [9–12]. Mg alloys containing Al and RE elements, such as AZ91 and WE43 alloys, showed a relatively high strength and good corrosion resistance. However, the biocompatibility of aluminum is poor. Al^{3+} ions can easily combine with inorganic phosphates, leading to a lack of phosphate in the human body; increased concentration of Al^{3+} in the brain seems to be associated with Alzheimer's disease [13]. In vivo studies showed that Nd and Y elements in WE43 mainly distributed at the implantation site after the degradation of magnesium implant [7]. In reality, there are only a small number of alloying elements that can be tolerated in the human body and can also retard the biodegradation of magnesium alloys: Ca, Zn, Mn, Si and perhaps very small amounts of low toxicity rare earth elements [14].

Recently, Hassel et al. [15] reported that calcium can improve both the corrosion resistance and mechanical properties of magnesium alloys in NaCl solution. Moreover, calcium is a major component in human bone and can accelerate its growth [16, 17]. Similar to calcium, zinc is an essential element in the human body and it has also an even more strengthening effect on magnesium alloys [18]. However, excessive amounts of zinc can be cytotoxic. This has been shown to be the case in Zn-doped calcium phosphates where more than $\sim$2 wt% appears to cause cytotoxicity [13]. Manganese is tolerable and essential to human body. Manganese has the function of refining grain size and improving tensile strength of magnesium alloys [19]. Similarly to manganese, silicon can be tolerated in the human body. A small content of Si has been reported to be essential in mammals [20].

Since according to Song [14] a Zn-containing magnesium alloy with small amounts of Ca, Mn or Si can be a potential biodegradable alloy, the present work aim at examining the bio-corrosion properties of Mg–Zn–Ca, Mg–Zn–Mn and Mg–Zn–Si alloys in a simulated physiological medium.

2 Experimental

Ternary Mg–Zn–X (X = Ca, Mn, Si) alloys of composition Mg–2Zn–0.2X (wt%) were prepared by direct synthesis from pure metals. Stoichiometric amounts of the constituents were placed in Ta crucibles which were arc sealed in order to avoid losses of high vapor pressure elements, such as Mg and Zn. Metals were melted in an induction furnace under argon flow. Samples containing Ca were weighed and sealed in the crucible inside a glove box to prevent oxidation. Small ingots with a diameter of about 0.8 cm were extracted from the crucibles.

The samples were tested in the as-cast condition. Scanning electron microscopy (SEM) and energy dispersive X-ray spectroscopy (EDXS) were used to examine microstructures and measure phase compositions prior electrochemical tests. A few alloys were prepared only for SEM-EDXS characterization, in order to check their homogeneity and global composition: in these cases both ingot sections, parallel and perpendicular to the crucible wall, were examined. A scanning electron microscope EVO 40 (Carl Zeiss) was used, equipped with a Pentafet Link (Oxford Instruments) detector for EDXS analysis. Smooth surfaces for microscopic observation before the electrochemical tests were prepared by using SiC papers and diamond pastes with grain size down to 1 μm. For the quantitative analysis an acceleration voltage of 20 kV was applied; a cobalt standard was used for calibration. The X-ray spectra were processed by the software package Inca Energy (Oxford Instruments).

Electrochemical experiments were performed in a standard three-electrode cell with 0.25 cm^2 of exposed area in the working electrode, having a platinum mesh as a counter electrode and a saturated calomel electrode (SCE) as reference. Working electrolyte was a naturally aerated aqueous Ringer's physiological solution (NaCl 9.00 g l^{-1}, $CaCl_2$ 0.24 g l^{-1}, KCl 0.43 g l^{-1}, $NaHCO_3$ 0.2 g l^{-1}). Prior to any immersion, the working electrodes were polished with 2400 grade silicon carbide paper and rinsed with distilled and ionized water. All experiments were carried out at 37°C, and the Mg–Zn–X alloys were studied in as-cast conditions, at different immersion times.

Potentiodynamic polarization studies were performed after 1 h of immersion in Ringer's solution for each alloy. Potentiodynamic polarization curves were recorded at a scan rate of 0.5 mV s^{-1} in the range from −2000 to −1000 mV vs. SCE, using a Solartron 1286 electrochemical interface.

Electrochemical impedance spectroscopy (EIS) measurements were carried out at open-circuit potential using a GAMRY EIS300 electrochemical frequency response analyzer (FRA) system. The impedance spectra were acquired in the frequency range from 10 kHz to 10 mHz with a perturbation signal of 10 mV. EIS spectra were acquired at different exposure times in the electrolyte. Scanning electron microscopy and electron probe microanalysis were used to investigate morphology and composition of the alloys' surface after the EIS measurements.

Table 1 SEM-EDXS data on Mg–2Zn–0.2X alloys

Alloy	Measured composition (wt%) Mg; Zn; X	Phases	Phases composition (wt%) Mg; Zn; X
Mg–2Zn–0.2Ca	97.4; 2.5; 0.1	(Mg) Mg–Zn phase containing Ca	99.2; 0.8; 0.0 96.8; 3.1; 0.1
Mg–2Zn–0.2Mn	97.8; 2.0; 0.2	(Mg) Mg–Zn binary phase	98.8; 1.0; 0.2 96.2; 3.7; 0.0
Mg–2Zn–0.2Si	97.3; 2.4; 0.3	(Mg) Mg–Zn binary phase Mg_2Si	98.9; 1.0; 0.1 94.6; 5.4; 0.0

For comparison, all tests were also performed on AZ91 magnesium alloy (Mg–9Al–1Zn, wt%) supplied by Johnson Matthey, London, UK. Measurements were performed thrice as to ensure reproducibility of results.

3 Results and discussion

3.1 Microstructural characterization

The microstructural, qualitative and quantitative analyses on the as cast samples highlight that the induction-melted ingots are homogeneous and their gross compositions correspond to the nominal ones. These results, obtained on several samples with the same nominal composition, confirm the validity of the preparation method used in this work.

The microstructure of all the Mg–2Zn–0.2X alloys is mainly formed by a Mg-based matrix. The matrix composition, as well as the presence of intermetallic phases in small amounts, depends on the alloying elements nature. Zinc, whose concentration is equal in all samples, is partially dissolved in the matrix, with concentration increasing from the centre to the border of grains, and partially localized in a white Mg–Zn intermetallic phase. According to the literature [21, 22] this phase should be identified as the $Mg_{21}Zn_{25}$ compound, even if its composition is difficult to measure accurately due to the distribution of this phase in small-sized crystals.

Each of the secondary alloying elements has a characteristic behaviour. In Mg–2Zn–0.2Ca alloys calcium is practically absent from the matrix (maximum 0.1 wt% at the grains border), being dissolved in the white Mg–Zn intermetallic phase. In Mg–2Zn–0.2Mn alloys manganese is homogeneously dissolved in the matrix, with average concentration corresponding to the nominal one. In Mg–2Zn–0.2Si alloys silicon is practically absent from the matrix (maximum 0.1 wt% at the grains centre), being localized in a white Mg–Si intermetallic phase which can be identified as Mg_2Si both from the approximate composition and from its characteristic "chinese script" morphology in the eutectic with Mg.

To summarize, alloys containing Ca and Mn are constituted by the same two phases: nevertheless Ca is localized in the intermetallic phase, on the contrary Mn is concentrated in the matrix. Alloy containing Si is constituted by three phases, with Si localized in the Mg_2Si intermetallic.

Results on phases analyses on the Mg-based matrix are listed in Table 1; qualitative analysis results allow the identification of intermetallic phases, but quantitative results are not shown, due to the small sizes of the measured regions. Each gross and matrix composition presented in Table 1 is a value averaged on at least six EDXS measurements on different spots. Representative microphotographs of the studied alloys are shown in Fig. 1a–c.

3.2 Electrochemical characterization

Figure 2 displays the polarization curves recorded after 1 h exposure to naturally aerated Ringer's physiological solution for AZ91 and Mg–2Zn–0.2X (X = Ca, Mn, Si) alloys. The cathodic polarization curves represent the cathodic process of water reduction with hydrogen release ($2H_2O + 2e^- \rightarrow 2OH^- + H_2$) [23–25] and are similar for all the tested alloys. The anodic polarization curves exhibit a knee point appearing at a certain potential value depending on the alloy composition. The anodic current density increases slowly with increasing polarization before the knee point and after which it increase rapidly. This indicates that there is a partially protective film on the alloys' surface to slow down the corrosion of substrate material. Such a surface film is mainly constituted by $Mg(OH)_2$ [26–28] and cannot be considered a real passive film owing to the significant anodic current density values measured below the knee point. Once the anodic potential reaches the knee point, the surface film fractures and the alloy substrate is corroded quickly. It can be assumed that all the tested alloys remain in a pseudopassive state over the range from the corrosion potential to the knee point, at which breakdown of the surface film occurs with a rapid increase in the current density.

The electrochemical parameters shown in Table 2 were obtained from the analysis of the polarization curves reported in Fig 2. As can be seen, the AZ91 alloy shows a better electrochemical behaviour compared to Mg–2Zn–0.2Si and Mg–2Zn–0.2Ca alloys being characterized by a higher value of the corrosion potential, E_{corr}, and

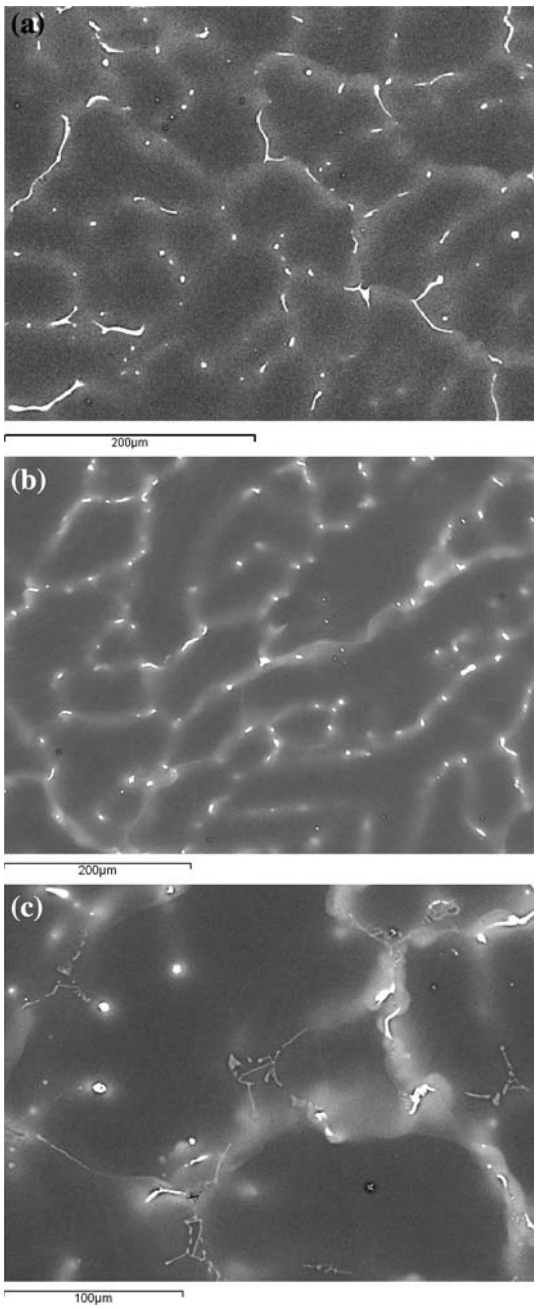

Fig. 1 Representative SEM micrographs of Mg–2Zn–0.2X alloys. **a** X = Ca; **b** X = Mn; **c** X = Si

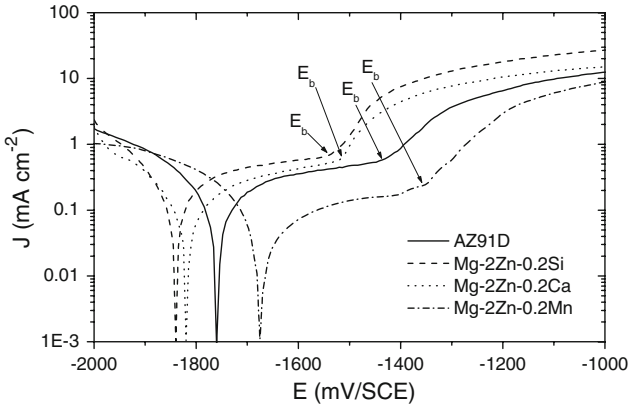

Fig. 2 Polarization curves of AZ91 and Mg–2Zn–0.2X (X = Ca, Mn, Si) alloys recorded after 1 h exposure to Ringer's physiological solution at 37°C

Table 2 Data obtained from polarization curves

Alloy	E_{corr} (mV/SCE)	E_b (mV/SCE)	i_{pp} (mA cm^{-2})
AZ91	−1760	−1450	0.35
Mg–2Zn–0.2Ca	−1820	−1520	0.45
Mg–2Zn–0.2Mn	−1680	−1360	0.15
Mg–2Zn–0.2Si	−1840	−1550	0.54

E_{corr} Corrosion potential, E_b breakdown potential, i_{pp} pseudopassivation current density

breakdown potential, E_b, and a lower value of the anodic current density in the pseudopassive range, i_{pp}. On the contrary, the E_{corr} value of Mg–2Zn–0.2Mn alloy is higher than that of AZ91 magnesium one. Moreover, Mg–2Zn–0.2Mn alloy exhibits a nobler value of E_b and a lower value of i_{pp} with respect to the AZ91 one, thereby indicating the formation of a more stable and protective film on its surface.

Corrosion damage results from electrochemical reactions, and electrochemical measurements can often reveal the corrosion mechanism. Electrochemical impedance spectroscopy (EIS) is a useful technique in the study of corrosion. The corrosion mechanism of magnesium sometimes can be estimated through analysing the measured electrochemical impedance spectrum [29, 30].

Figure 3 is representative of the impedance diagrams, obtained at the open circuit potential for AZ91 and Mg–2Zn–0.2X (X = Ca, Mn, Si) alloys directly exposed to the naturally aerated Ringer's physiological solution. In all cases, the electrochemical impedance spectra apparently exhibit a single capacitive loop at all frequencies, whose diameter depends on the composition of the tested alloys, and on the exposure time. The diameter of the capacitive loop is related to the corrosion rate. Makar et al. [31] compared corrosion rates calculated from the first capacitive loop in the high frequency region with weight loss results for a range of magnesium alloys, and found that most of the EIS results matched very well with the weight loss data. All the tested alloys exhibit similar EIS spectra, except for the difference in the diameter of the capacitive loop. This means that the corrosion mechanism of these alloys is the same, but their corrosion rate is different. As can be seen, increasing exposure time to the aggressive solution leads to a decrease in the diameter of the capacitive loop which means a decrease in corrosion resistance.

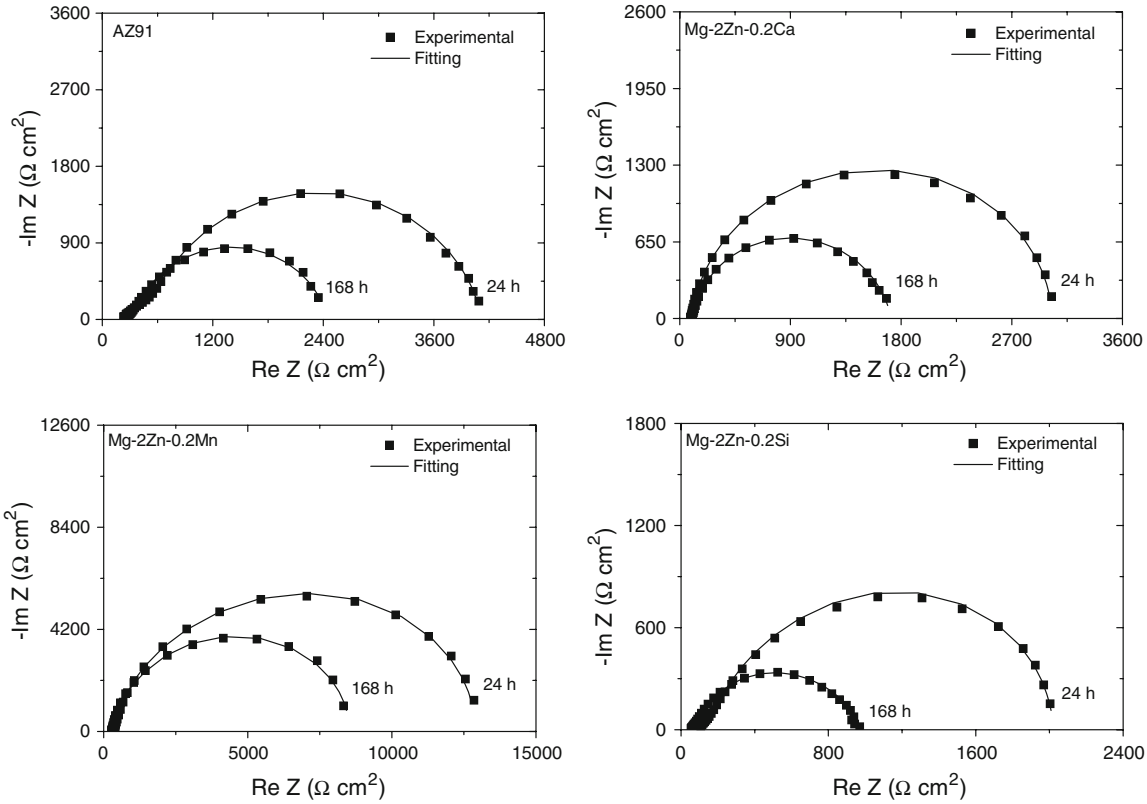

Fig. 3 Representative impedance spectra of AZ91 and Mg–2Zn–0.2X (X = Ca, Mn, Si) alloys in Ringer's physiological solution at 37°C

In order to enable an accurate analysis of the impedance diagrams the equivalent circuit model reported in Fig. 4 was used. This equivalent circuit contains a solution resistance, R_s, and two elements in series: (i) a charge transfer resistance of the corrosion process on the metal surface, R_{ct}, in parallel with a double-layer capacitance, C_{dl}, and (ii) a film capacitance, C_f, in parallel with a film resistance, R_f [32–34]. On the other hand, the polarization curves results (Fig. 2) proved the existence of a $Mg(OH)_2$ surface film on the tested alloys. A very good agreement between experimental and theoretical data was obtained. The standard deviation χ-quadrate was in the order of 10^{-5}, and the relative error was less than 5%.

Figure 5 reports, for the different alloys, the variation of the polarization resistance, R_p, as a function of exposure time to the aggressive solution. The polarization resistance of each alloy was calculated by adding its R_{ct} and R_f values [35, 36]. The corrosion rate is inversely related to R_p—the higher the value of R_p the higher the corrosion resistance (lesser corrosion rate). For all alloys it can be seen that R_p decreases with increasing exposure time, indicating a worsening of corrosion behaviour. This can be ascribed to a progressive weakening of the protective performance of surface film owing to the attack of chloride ions with

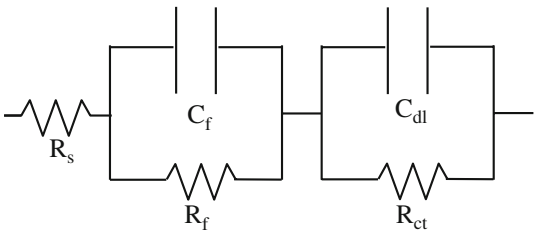

Fig. 4 Equivalent circuit model used for fitting the experimental EIS data

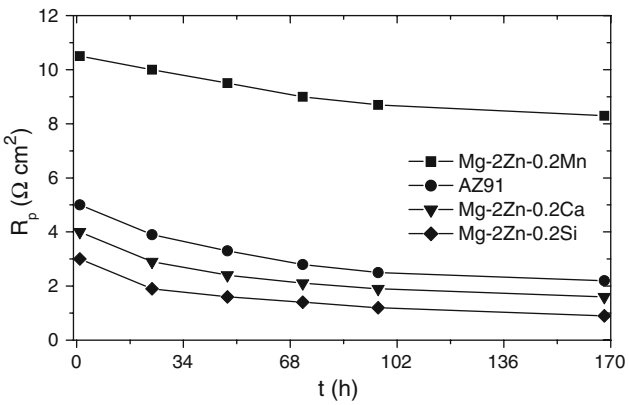

Fig. 5 Variation of polarization resistance, R_p, for AZ91 and Mg–2Zn–0.2X (X = Ca, Mn, Si) alloys as a function of exposure time to Ringer's physiological solution

consequent fast dissolution reaction of the magnesium substrate. The results are in line with those obtained from polarization measurements. As a matter of fact, the AZ91 alloy exhibits better corrosion resistance compared to Mg–2Zn–0.2Si and Mg–2Zn–0.2Ca alloys being characterized by higher R_p values on the entire exposure period at the aggressive environment. On the contrary, Mg–2Zn–0.2Mn alloy exhibits significantly higher R_p values compared to the AZ91 one. Higher R_p values are indicative of reduced dissolution rates confirming the better corrosion resistance of Mg–2Zn–0.2Mn alloy as a consequence of the improved properties of surface film.

After 168 h exposure to the Ringer's physiological solution the alloys surface is covered with a layer of corrosion products (Fig. 6), mainly constituted by Mg, O and Cl, as revealed by EDXS microanalysis, indicating an almost uniform corrosive attack [33, 34, 37].

When the samples are exposed to the corrosion medium (Ringer's physiological solution), chemical dissolution and electrolyte penetration result in spontaneous corrosion on the entire surface leading to fast degradation rates of the magnesium surface. One by-product of magnesium dissolution is the OH^- ion which can promote precipitation of $Mg(OH)_2$ (brucite) whose crystal structure is hexagonal close packed. The Cl^- ions present in the aggressive environment can easily penetrate the hydroxide film thus accelerating the dissolution of the substrate owing to the formation of a basic chloride salt which is readily accommodated in the layer structure of $Mg(OH)_2$ [38–40].

Microstructural characterization of the Mg–2Zn–0.2Mn alloy evidenced the presence of manganese in solid solution with the magnesium matrix and this is believed to have a favourable effect on its corrosion behaviour. As matter of fact, the surface film covering Mn-containing magnesium alloys has been shown to contain an appreciable fraction of manganese oxides/hydroxides [41, 42]. These oxides/hydroxides are expected to enhance the surface passivity [41]. Therefore, the improved corrosion resistance of the Mg–2Zn–0.2Mn alloy compared to the AZ91 one can be triggered by incorporation of oxidized manganese in the brucite layered structure, via substitution of the magnesium cations, to hinder incorporation of chloride anions in the $Mg(OH)_2$ lattice, so enhancing the protective performance of the surface film.

Based on hydrogen evolution rate (which is proportional to the metal dissolution or corrosion rate) Song [14] has suggested that a potential magnesium-based implant should possess six times lower hydrogen evolution rate than AZ91 alloy. When comparing the present electrochemical experimental results of Mg–2Zn–0.2Mn alloy with AZ91 one the improvement in the corrosion resistance achieved can be considered encouraging. EIS results reveal that the polarization resistance of Mg–2Zn–0.2Mn alloy after 168 h exposure to the Ringer's solution is about four times higher than AZ91 alloy. It is noted that though previous in vivo studies showed no toxic effects due to dissolution of AZ91 alloy (containing 9% aluminum) aluminum toxicity in human body is a known fact [13, 43]. The present study suggests that the Mg–2Zn–0.2Mn alloy could be a promising candidate for its application in degradable orthopedic implants, and it is worthwhile to further investigate the in

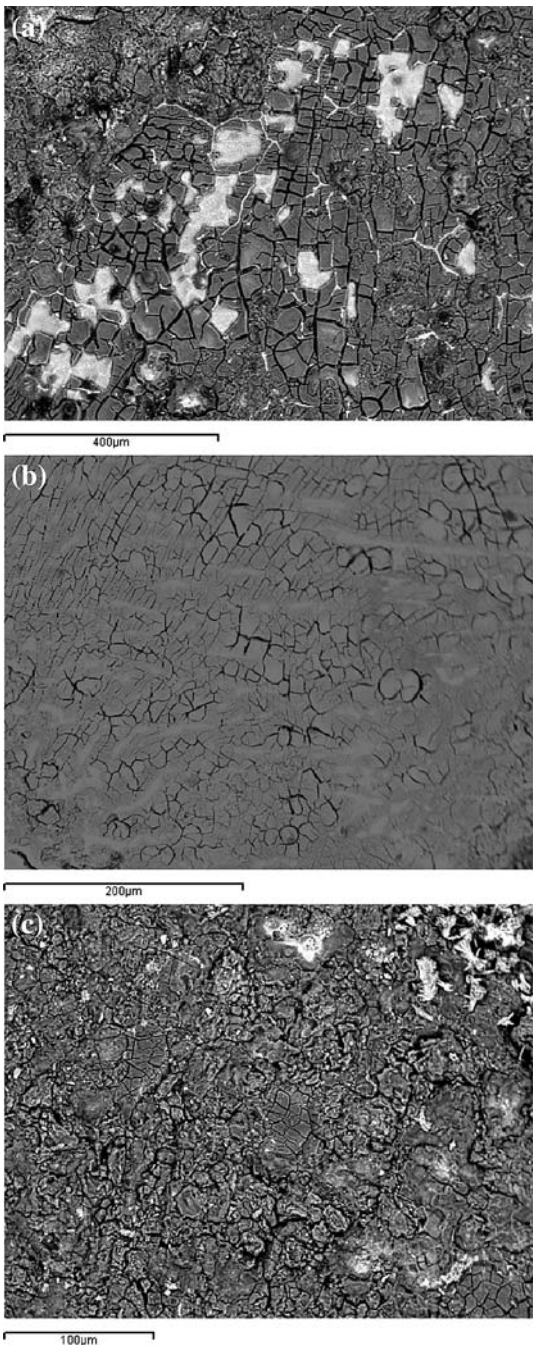

Fig. 6 SEM micrographs of Mg–2Zn–0.2X alloys surface after 168 h exposure to Ringer's physiological solution at 37°C. **a** X = Ca; **b** X = Mn; **c** X = Si

vivo behaviour of this alloy as well as to assess its mechanical properties for this specific purpose.

4 Conclusion

The bio-corrosion behaviour of Mg–2Zn–0.2X (X = Ca, Mn, Si) alloys was investigated in Ringer's physiological solution and compared with that of the AZ91 magnesium alloy. Potentiodynamic polarization and electrochemical impedance spectroscopy results shows a better corrosion behaviour of the AZ91 alloy with respect to Mg–2Zn–0.2Ca and Mg–2Zn–0.2Si alloys. On the contrary, a significantly enhanced corrosion resistance is observed for the Mg–2Zn–0.2Mn alloy compared to the AZ91 one: Mg–2Zn–0.2Mn alloy exhibits a four-fold increase in the polarization resistance than AZ91 alloy after 168 h exposure to the Ringer's physiological solution. The improved corrosion behaviour of the Mg–2Zn–0.2Mn alloy with respect to the AZ91 one can be ascribed to enhanced protective properties of the $Mg(OH)_2$ (brucite) surface layer due to the incorporation of oxidized manganese in the brucite layered structure.

References

1. Ducheyne PL, Hasting GW. Functional behaviour of orthopedic biomaterials applications, vol 2. Boca Raton, FL: CRC Press; 1984. p. 3.
2. Davis JR. Handbook of materials for medical devices. USA: ASM International; 2003.
3. Zhang E, Xu L, Yang K. Formation by ion plating of Ti-coating on pure Mg for biomedical applications. Scripta Mater. 2005;53:523–7.
4. Hofmann GO. Biodegradable implants in traumatology: a review on the state-of-the-art. Arch Orthop Trauma Surg. 1995;143: 123–32.
5. Vormann J. Magnesium: nutrition and metabolism. Mol Aspects Med. 2003;24:27–37.
6. Miller PL, Shaw BA, Wendt RG, Moshier WC. Assessing the *corrosion* resistance of nonequilibrium Mg-Y alloys. Corrosion. 1995;51:922–31.
7. Witte F, Kaese V, Haferkamp H, Switzer E, Meyer-Lindenberg A, Wirth C, et al. In vivo corrosion of four magnesium alloys and the associated bone response. Biomaterials. 2005;26:3557–63.
8. Song G, Song S. A possible biodegradable magnesium implant material. Adv Eng Mater. 2007;9:298–302.
9. Witte F, Fischer VJ, Nellsen J, Crostack H-A, Kaese V, Pisch A, et al. In vitro and in vivo corrosion measurements of magnesium alloys. Biomaterials. 2006;27:1013–8.
10. Liu C, Xin Y, Tian X, Chu PK. Degradation susceptibility of surgical magnesium alloy in artificial biological fluid containing albumin. J Mater Res. 2007;22:1806–14.
11. Kannan MB, Singh Raman RK. In vitro degradation and mechanical integrity of calcium-containing magnesium alloys in modified-simulated body fluid. Biomaterials. 2008;29: 2306–14.
12. Quach N-C, Uggowitzer PJ, Schmutz P. Corrosion behaviour of an Mg–Y–RE alloy used in biomedical applications studied by electrochemical techniques. C.R. Chimie. 2008;11:1043–54.
13. Lucey TD, Venugopal B. Metal toxicity in mammals. New York: Plenum Press; 1977.
14. Song G. Control of biodegradation of biocompatable magnesium alloys. Corros Sci. 2007;49:1696–701.
15. Hassel T, Bach F-W, Golovko A, Krause C. Magnesium technology in the global age. In: 45th annual conference of metallurgists of CIM, Montreal, Quebec, Canada; 2006, pp. 359–370.
16. Ilich JZ, Kerstetter JE. Nutrition in bone health revisited: a story beyond calcium. J Am Coll Nutr. 2000;19:715–37.
17. Serre CM, Papillard M, Chavassieux P, Vogel JC, Boivin G. Influence of magnesium substitution on a collagen-apatite biomaterial on the production of a calcifying matrix by human osteoblasts. J Biomed Mater Res. 1998;42:626–33.
18. Boehlert CJ, Knittel K. The microstructure, tensile properties, and creep behavior of Mg–Zn alloys containing 0–4.4 wt% Zn. Mater Sci Eng A. 2006;417:315–21.
19. Khan SA, Miyashita Y, Mutoh Y, Bin Sajuri Z. Influence of Mn content on mechanical properties and fatigue behavior of extruded Mg alloys. Mater Sci Eng A. 2006;420:315.
20. Underwood EJM. Elements in human and animal nutrition. 4th ed. New York: Academic; 1977.
21. Ĉerny R, Renaudin G. Acta Cryst. 2002;C58:154.
22. Barcon A, Brunskill APJ, Lalancette RA, Thompson HW. (±)-3-Oxocyclohexanecarboxylic and -acetic acids: contrasting hydrogen-bonding patterns in two homologous keto acids. Acta Cryst. 2002;C58:154–6.
23. Hallopeau X, Beldjoudi T, Fiaud C, Robbiola L. Corros Rev. 1998;16:27.
24. Pebere N, Riera C, Dabosi F. Investigation of magnesium corrosion in aerated sodium sulfate solution by electrochemical impedance spectroscopy. Electrochim Acta. 1990;35:555–61.
25. Ardelean H, Frateur I, Marcus P. Corrosion protection of magnesium alloys by cerium, zirconium and niobium-based conversion coatings. Corros Sci. 2008;50:1907–18.
26. Song G, Atrens A, StJohn D, Nairn J, Li Y. The electrochemical corrosion of pure magnesium in 1 N NaCl. Corros Sci. 1997;39:855–75.
27. Bonora PL, Andrei M, Eliezer A, Gutman EM. Corrosion behaviour of stressed magnesium alloys. Corros Sci. 2002;44:729–49.
28. Nordlien JH, Nisancioglu K, Ono S, Masuko N. Morphology and structure of oxide films formed on MgAl alloys by exposure to air and water. J Electrochem Soc. 1996;143:2564–72.
29. Song G, Atrens A, StJohn D, Wu X, Nairn J. The anodic dissolution of magnesium in chloride and sulphate solutions. Corros Sci. 1997;39:1981–2004.
30. Song G, Atrens A, Wu X, Zhang B. Corrosion behaviour of AZ21, AZ501 and AZ91 in sodium chloride. Corros Sci. 1998;40:1769–91.
31. Makar GL, Kruger J, Joshi A. In: Paris HG, Hunt WH, editors. Advances in magnesium alloys and composites, Warrendale, PA: TMS; 1988, p. 105.
32. Baril G, Pebere N. The corrosion of pure magnesium in aerated and deaerated sodium sulphate solutions. Corros Sci. 2001;43:471–84.
33. Baril G, Blanc C, Pebere N. AC impedance spectroscopy in characterizing time-dependent corrosion of AZ91 and AM50 magnesium alloys characterization with respect to their microstructures. J Electrochem Soc. 2001;148:B489–96.
34. Baril G, Galicia G, Deslouis C, Pebere N, Tribollet B, Vivier V. An impedance investigation of the mechanism of pure magnesium corrosion in sodium sulfate solutions. J Electrochem Soc. 2007;154:C108–13.

35. Jin S, Amira S, Ghali E. Electrochemical impedance spectroscopy evaluation of the corrosion behavior of die cast and thixocast AXJ530 magnesium alloy in chloride solution. Adv Eng Mater. 2007;9:75–83.
36. Kannan MB, Raman RKS. In vitro degradation and mechanical integrity of calcium-containing magnesium alloys in modified-simulated body fluid. Biomaterials. 2008;29:2306–14.
37. Zucchi F, Grassi V, Frignani A, Monticelli C, Trabanelli G. Electrochemical behaviour of a magnesium alloy containing rare earth elements. J Appl Electrochem. 2006;36:195–204.
38. Godard HP, Jepson WB, Bothewell MR, Kane RL. The corrosion of light metals. New York: Wiley; 1967. p. 260.
39. Song G, Atrens A. Corrosion mechanisms of magnesium alloys. Adv Eng Mater. 1999;1:11–33.
40. Song G, Atrens A. Understanding magnesium corrosion-a framework for improved alloy performance. Adv Eng Mater. 2003;5:837–58.
41. Anderson WA, Stumpf HC. Effects of manganese on the electrode or free corrosion potentials of aluminum. Corrosion. 1980;36:212–3.
42. Lunder O, Akune TKR, Nisancioglu K. Effect of manganese additions on the corrosion behavior of mould-cast magnesium ASTM AZ91. Corrosion. 1987;43:291–5.
43. Ganrot PO. Metabolism and possible health effects of aluminum. Environ Health Perspect. 1986;65:363–441.